Title

High-performance detection of somatic D-loop mutation in urothelial cell carcinoma patients by polymorphism ratio sequencing

Journal

Journal of Molecular Medicine, 94(9)

ISSN

0946-2716

Authors

Duberow, David P
Brait, Mariana
Hoque, Mohammad O
et al.

Publication Date

2016-09-01

DOI

10.1007/s00109-016-1407-2

Peer reviewed

HHS Public Access

Author manuscript

J Mol Med (Berl). Author manuscript; available in PMC 2022 February 28.

Published in final edited form as:

J Mol Med (Berl). 2016 September ; 94(9): 1015–1024. doi:10.1007/s00109-016-1407-2.

High-performance detection of somatic D-loop mutation in urothelial cell carcinoma patients by polymorphism ratio sequencing

David P. Duberow[1,6], **Mariana Brait**[2], **Mohammad O. Hoque**[2], **Dan Theodorescu**[3,4], **David Sidransky**[2], **Santanu Dasgupta**[5], **Richard A. Mathies**[1]

[1] Department of Chemistry, University of California, 307 Lewis Hall, Berkeley, CA 94720, USA

[2] Department of Otolaryngology—Head and Neck Surgery, Head and Neck Cancer Research Division, Johns Hopkins University School of Medicine, Baltimore, MD 21231, USA

[3] Department of Pharmacology, University of Colorado Comprehensive Cancer Center, Aurora, CO 80045, USA

[4] Department of Surgery (Urology), University of Colorado Comprehensive Cancer Center, Aurora, CO 80045, USA

[5] Department of Cellular and Molecular Biology, The University of Texas Health Science Center at Tyler, Tyler, TX, USA

[6] Present address: Department of Chemistry, City College of San Francisco, 50 Phelan Ave., San Francisco, CA 94112, USA

Abstract

Utilizing a polymorphism ratio sequencing platform, we performed a complete somatic mutation analysis of the mitochondrial D-loop region in 14 urothelial cell carcinomas. A total of 28 somatic mutations, all heteroplasmic, were detected in 8 of 14 individuals (57.1 %). Insertion/deletion changes in unstable mono- and dinucleotide repeat segments comprise the most pervasive class of mutations (9 of 28), while two recurring single-base substitution loci were identified. Seven variants, mostly insertion/deletions, represent population shifts from a heteroplasmic germline toward dominance in the tumor. In four cases, DNA from matched urine samples was similarly analyzed, with all somatic variants present in associated tumors readily detectable in the bodily fluid. Consistent with previous findings, mutant populations in urine were similar to those detected in tumor and in three of four cases were more prominent in urine.

✉ Santanu Dasgupta santanu.dasgupta@uthct.edu, Richard A. Mathies ramathies@berkeley.edu.

Author contribution R.A.M., S.D., and D.S. designed the experiments. D.P.D. and M.B. performed research. R.A.M., S.D., D.S., M.O.H., D.P.D., and D.T. analyzed the data and provided materials. R.A.M., S.D., and D.S. designed the project, supervised research. R.A.M., S.D., D.S., M.O.H., D.P.D., D.T., and M.B. wrote the paper.

Compliance with ethical standards

Conflict of interest statement R.A.M. has a financial interest in a company (IntegenX Inc.) working on the commercialization of microchip sequencing technologies that may benefit from the results of this research. Others have declared no competing interest.

Keywords

mtDNA; Urothelial cell carcinoma; Polymorphism ratio sequencing; Somatic mutation; D-loop

Introduction

Historically known as the powerhouse of the cell, the mitochondrion (mt) plays a powerful and paradoxical role in cell survival and proliferation. In addition to providing over 80 % of the cell's energy through oxidative phosphorylation (OXPHOS), the mt also participates in the synthesis of such biomolecular building blocks as amino acids, phospholipids, and heme. More morbidly, permeation of the outer mt membrane in response to intracellular signaling cascades is a key step in apoptosis, the suicide pathway by which irreparably damaged cells are eliminated and tissue proliferation is restricted [1]. Mitochondrial dysfunction has been suspected as a major factor in tumor onset and progression since as early as Warburg [2], and recent years have seen experimental confirmation of altered mt content and function in human cancer [3].

In addition to harboring key metabolic machinery, the mt also contains its own compact, circular genome of 16,569 bp. The mitochondrial DNA (mtDNA) encodes 22 tRNAs, 2 rRNAs, and 13 proteins, all of which form functional subunits in mitochondrial OXPHOS structures [3]. Additionally, a non-coding control region contains promoters and other factors regulating transcription [3]. In the past decade, somatic mutations in the mtDNA have been uncovered in a wide range of cancers, including head and neck, breast, kidney, liver, colorectal, pancreatic, bladder, and lung [3]. More recently, the functional role of these mutations has begun to come into focus, with the demonstration of increased tumor growth and metastasis in the presence of coding mutations [4–6].

The exploitation of mtDNA sequence variation as a viable tool in cancer detection and characterization presents a variety of unique benefits and challenges. The relative abundance of the mtDNA, hundreds to thousands of copies per cell, makes the genome an attractive target for genetic analysis, enabling the acquisition of high-quality data from minimal sample. In addition, its proximity to the reactive oxygen species (ROS) generated as by-products of electron transport renders the mtDNA more susceptible to damage and subsequent mutation, providing a direct window for observing the cycle of oxidative damage believed to be implicated in a variety of mitochondrial diseases [7–9]. More problematic is the issue of heteroplasmy, the phenomenon by which multiple genetic populations may exist within a single cell as a result of mitochondrial multiplicity [3]. While tracking heteroplasmy shifts over time may ultimately prove useful in monitoring tumor progression, assigning numerical significance to these changes is difficult with conventional sequencing, hybridization, and PCR-based technology due to the nonlinearity and extensive data processing associated with these techniques.

Earlier, we introduced polymorphism ratio sequencing (PRS), a Sanger sequencing-based technique that allows for direct and quantitative determination of sequence variation [10]. Utilizing this technology, in this report, we detail the application of microchip-based PRS analysis to the high-throughput detection of somatic mtDNA variants in a pool of 14

primary tumor tissues samples obtained from urothelial cell carcinoma (UCC) patients. The UCC provides a useful model system by virtue of its relatively high incidence, being the seventh most common in the USA, with an estimated 74, 000 new cases and 16,000 deaths in 2015 [11]. A high frequency of mtDNA mutations has also been established in UCC (at least one somatic mutation in >50 % of all cases screened) [12, 13]. Additionally, the relative ease with which an associated bodily fluid can be collected presents a unique opportunity for routine screening and early detection, should reliable biomarkers be detectable in urine. In all cases screened here, mtDNA extracted from matched lymphocytes serves as a normal internal control by which tumor-associated mutations are differentiated from germline polymorphisms. The analysis of available matched urine mtDNA is also explored to investigate the use of bodily fluids as potential non-invasive indicators of tumor infiltration or recurrence under a PRS analysis scheme. The results obtained here highlight the advantages of PRS as a technique for sensitive, high-throughput mutation detection in clinical samples.

Materials and methods

Microfabrication

The design and fabrication of the μCAE device have been described previously [14–16]. Briefly, the device consists of 96 separation capillaries arrayed radially on a 150-mm Borofloat glass wafer and converging on a common anode. Each capillary is 17 cm long, 200 μm wide, and 30 μm deep. Adjacent capillaries are coupled by common cathode and waste reservoirs, forming 48 doublets, each with a common injection structure. Microchannel features are formed by isotropic wet etching with concentrated HF and sealed by thermally bonding a second blank wafer to the channel layer. Fluidic access ports are diamond-drilled into the etched layer. A final layer of 1/8-in.-thick Borofloat rings replacing the PMMA buffer moats previously employed [15] is attached to the top of the device in a second thermal bonding step.

Sample acquisition and quantitation

After initial patient de-identification, all original histologic slides from 14 UCC tissue specimens were reviewed by a senior pathologist to reconfirm the diagnosis. All histologic slides were obtained from formalin-fixed, paraffin-embedded tissue. Prior to DNA extraction, slides were microdissected to obtain >70 % neoplastic cells. Genomic DNA was extracted from microdissected tumor tissues, matched lymphocytes, and urine sediments using phenol/chloroform followed by ethanol precipitation, as described previously [17, 18]. Following transfer of fully extracted samples to UC Berkeley, all solutions were quantitated using the PicoGreen assay (Invitrogen, Carlsbad CA) and the grouping by individual verified by PowerPlex 16 STR genotyping analysis (Promega, Madison WI).

Template amplification

Generation of template for PRS extension was performed by PCR amplification of the entire mitochondrial displacement loop (D-loop) in two overlapping fragments of lengths 765 and 954 bp. Total DNA template (10 ng) was combined with 7.5 pmol each of forward and reverse PCR primer (Integrated DNATechnologies, Coralville IA), 2.5 μL of 10× PCR buffer

(-$MgCl_2$), 0.5 nmol of each dNTP, 37.5 nmol of $MgCl_2$, and 1.25 U of Platinum TAQ DNA polymerase (Invitrogen) and diluted to a total reaction volume of 25 μL with nuclease-free water (ISC BioExpress, Kaysville, UT). PCR primer sets 23 and 24 from Rieder et al. [19]. were modified at the 5′ end to include universal sequencing primer recognition (−40 M13 for forward and −28 M13 for reverse primers). PCR reactions were incubated in an MJ Research PTC-200 thermal cycler for 30 cycles of denaturation (94 °C for 30 s), annealing (61 °C for 45 s), and extension (72 °C for 90 s). The thermal program was initiated with a 60-s denaturation at 94 °C and terminated with a final extension at 72 °C for 180 s.

PCR products were purified enzymatically by incubation with 30 U of exonuclease I and 2 U of shrimp alkaline phosphatase (GE Healthcare, Piscataway, NJ) for 30 min at 37 °C, followed by 15 min at 80 °C. Products were quantitated by PicoGreen and diluted to a final concentration of 12 ng/μL.

PRS extension and pooling

Sanger extension is performed using energy transfer (ET) dye primer labeling chemistry and has been reported previously in detail. For each uniquely labeled set of extension fragments, 4 μL (48 ng) of purified PCR product was combined robotically with 800 fmol (2 μL of 400 nM) of the appropriate universal ET sequencing primer (FAM-R110, FAM-R6G, FAM-TAMRA, and FAM-ROX, with emission maxima 525, 555, 580, and 605 nm, respectively) [20] and 2 μL of DYEnamic Direct Cycle Sequencing Mix (GE Healthcare). The reactions were then diluted with water to a total volume of 10 μL. Thermal cycling consisted of 45 cycles of denaturation (95 °C for 30 s), annealing (52 °C for 15 s), and extension (72 °C for 60 s). Extension fragments were pooled and purified by co-precipitation with 15 μg of glycogen (MP Biomedicals, Solon, OH) in 3 μL of 7.5 M ammonium acetate (Fisher, Pittsburgh, PA) and 110 μL of 100 % ethanol (Rossville, Hayward, CA). After 60 min at −4 °C, the reactions were centrifuged at 3,700 rpm for 30 min and the pellets washed with 150 μL of 70 % ethanol. The pellets were recollected by a second 5-min centrifugation at 3,700 rpm and allowed to air dry before resuspension in 15 μL of 50 % HiDi Formamide (Applied Biosystems, Foster City, CA).

Microchip preparation and operation

Prior to analysis, microchannels were coated using a modified Hjertén procedure [21]. Channels were primed with 1 mL of 1× TTE (50 mM tris, 50 mM TAPS, 1 mM EDTA, pH 8.3), and the separation matrix (GenomeLab Separation Gel LPA-1, Beckman-Coulter, Fullerton, CA) was loaded via the central anode using a high-pressure gel loader [22]. Excess matrix was evacuated from the sample reservoirs and 1.8 μL of the sample was added to each well. The microdevice was then transferred to the Berkeley Confocal Rotary Scanner [23], where a ring bearing 96 electrodes was affixed to the sample reservoirs. Cathode, anode, and waste moats were filled with 5× TTE buffer and electrical connections were applied to each. PRS fragments were injected electrokinetically at 30 V/cm for 270 s, followed by separation at 150 V/cm for 30 min. Both the injection and separation were performed at 67 °C.

Data analysis

Following data collection, electropherograms were processed using an automated MATLAB-based data analysis program. Raw electropherograms were first truncated, leaving only data between 7 and 27 min in the trace and removing primer and PCR runoff peaks. Data were baseline-corrected with a dynamic top-hat algorithm, and spectral deconvolution was performed using four-color peak intensities from a PCR-generated ET primer standard. Following global normalization of signal intensities, a dynamic time warp algorithm was employed to align normal and tumor traces temporally using maximal overlap in non-variant regions to define a unique quality score at each data point. Squared difference maxima exceeding three standard deviations were identified automatically as possible mutations. Secondary inspection of these regions using sequence context and four-color peak signature confirmed the presence of authentic variants. Genetic populations were quantified using relative peak areas, with variants in low-resolution mononucleotide repeats estimated assuming equal contribution of all bases in the repeat. All mutations were confirmed by conventional sequencing.

Results

In this study, we have utilized PRS technology with a modified coding and pooling scheme depicted in Fig. 1. In separate reaction vessels, Sanger extension fragments corresponding to the same terminating base are labeled with distinct dye primers identifying the template. These fragments are then pooled and separated electrophoretically, yielding an electropherogram that overlaps perfectly in all places, except in instances of variation. Monitoring the squared difference between corresponding traces provides a direct indication of variant location, producing a nonzero value only in regions of poor overlap. Moreover, the inclusion of an internal control provides a standard for variant quantitation, with peak ratios linear in genotype population to a detection limit of 5 % mutant frequency. With four-color detection capabilities, two bases (by convention, A/C and G/T) may be monitored simultaneously. The coupling of A/C and G/T requires multiple trace correlation to confirm single-base transitions, the most common mutation class, building in a layer of redundancy and reducing the effects of single-sample anomalies [10]. In initial validations, labeled and pooled fragments were analyzed on a 96-lane microfabricated capillary array electrophoresis (μCAE) bioprocessor. In addition, the microfabricated platform lends itself well to integration [24–26] and parallelization [14, 15, 23, 27], thus decreasing operational intensity while increasing throughput.

Utilizing this improvised platform, we have analyzed the D-loop mtDNA regions in 14 primary UCC tumors. Comprehensive variant data are compiled in Table 1. Of 14 individuals with verifiably complete sample sets, 8 (57 %) harbored at least one somatic D-loop mutation (Table 1). As confirmed by MITOMAP, the online mtDNA database [28], 12 of these variants are novel somatic mutations previously unreported in the literature. Consistent with previous D-loop mutation analyses, the most pervasive mutations between individuals were insertion/deletion changes in unstable repeat segments, notably the D310 tract (base positions 303–315) and the poly-C region from 16184 to 16193. Some degree of heteroplasmy is evident in all 28 variants, appearing in both single-base substitutions and

insertion/deletion variants. Among these, seven mutations occurring in samples 6 and 13 appear to be population shifts from an already heteroplasmic germline. Where detected in the associated tumor, somatic mutations were also detected in urine, although to varying degrees. In a majority of samples (three of four), these changes were more pronounced in urine than in the tumor itself, appearing as heteroplasmies biased more strongly toward the mutant genotype. The perfect correlation between mutation sites detected in the tumor and urine in all four instances of available urine also serves as confirmation that these mutations are authentic and not due to “field cancerization” effects arising from formalin fixation [29]. With a total of 15 somatic variants, sample 6 was by far the most frequently mutated individual (Table 1). Selected representative data from this set are illustrated in Fig. 2. In addition to single-base deletions in both major poly-C tracts, 12 transition substitutions, all heteroplasmic, are present. Of these variants, 10 occur in closely grouped mutation clusters, forming three pairs of two adjacent transitions at TG152, AC225, and AG15927, as well as four mutations within 21 bases of the poly-C tract at 16184. Shifts from germline heteroplasmy toward a homoplasmic tumor account for all three non-transition mutations (C303del, C16183→A, and C16187del). Notably, many of the mutation sites for this sample (7 of 15) were germline polymorphic relative to the Revised Cambridge reference sequence [30] and may be indicative of a high-risk mitochondrial haplotype.

In nearly all cases of insertion/deletion in the poly-C tract at 16184, conventional sequencing reveals a range of up to five genetic populations, each differing by a single C insertion, in all biological sources including blood. Although these individual populations are invisible to PRS, the average differences between normal, tumor, and urine appear clearly as a single variation followed by a perfect overlap between subsequent regions in the trace, as illustrated in Fig. 3. Curiously, such vast population distributions were typically not observed in D310 alterations: conversely, heteroplasmic insertion/deletions were distributed between a single normal and single mutant genotype.

Also noteworthy among mutated individuals is sample 13, in which a germline-heteroplasmic two-base insertion/deletion between the CA514 dinucleotide repeat and the D310 tract is corrected almost perfectly in the tumor. The PRS traces containing the double indel are illustrated in Fig. 4, the mutation appearing as a series of minor normal pre-peaks occurring before the more intense dominant peaks, traceable by the tumor tracks between the CA insertion at 514 and the CC deletion at 303. This variant is particularly difficult to detect and characterize even by PRS, as complete data analysis requires the recognition and extraction of a systematic trend relative to the expected track, which in this example is represented by a homoplasmic tumor.

Discussion

The observation of heteroplasmy in 100 % of detected mutants is perhaps the most striking result of this study. The phenomenon of mt heteroplasmy presents unique opportunities for understanding the acquisition of mutations in a greater pathological scheme; however, it also presents similarly unique challenges to reliable detection and quantitation [3]. Beyond the prevalence of heteroplasmy, the recurrence of several mutation sites in the results obtained here is noteworthy. By far, single- or double-C insertion/deletion mutations

in the poly-C repeat at 16184 (five individuals) and the D310 tract (three cases), most likely due to polymerase error accumulation during replication, were the most common recurring variants. The observation of multiple genetic populations at C16184, even in germline DNA, is curious, especially considering the lack of such complexity at the highly variable D310 tract. This asymmetry may be related to the presence of a common T16189→C polymorphism in most mutated individuals, producing the longest uninterrupted mononucleotide repeat in the D-loop (10C compared to 7C and 5C in the D310 tract). In addition, two single-base substitutions, A16183→C and T16223→C, each appear in two individuals. It is noteworthy that A16183→C represents the lone transversion observed in these results; however, its adjacency to the repeat at C16184, also mutated in both cases, is a more likely contribution to its relatively high mutation frequency. Of note, compared to our previous study [12], we have detected higher frequency of mtDNA mutation (57 vs. 30 %) using the PRS technology.

Owing to its uncommonly high mutation frequency and the variety in detected alterations, sample 6 represents an interesting, singular example of the nature of mitochondrial mutations observed in UCC. In addition to the sheer number of variants (1 % mutation rate due to the cancer alone), the mutations detected in this sample are universally heteroplasmic, with three representing shifts in germline heteroplasmy to a homoplasmic tumor. The high proportion of heteroplasmic drift observed in this sample is consistent with a model of mtDNA mutation accumulation originating from enhanced ROS generation by a damaged electron transport chain. This model has garnered recent support through functional studies establishing the contribution of somatic mutations in complexes I and II to ROS production and enhanced tumorigenic phenotypes in cell culture models [4, 6, 31, 32]. Additionally, the presence of multiple mutation clusters at TG152, AC225, AG15927, and the poly-C tract at 16184 may be indicative of particular damage events, possibly from these endogenous mutagens, affecting multiple bases locally. While insufficient to establish functional relevance, the detection of five alterations within the heavy-strand origin—three in highly conserved regions—suggests a potential effect on replication efficiency. More interestingly, the double transition at AG15927 occurs in the tRNA threonine gene, 96 bp outside of the control region. The detection of these variants in the modest fraction of coding sequence (450 bp) spanned by the PCR amplicons employed here corroborates previous findings of somatic mtDNA-coding mutations in cancer [33–42] and suggests their presence at a reasonably high frequency. Complete mtDNA sequencing in coding regions may thus uncover an even greater number of mutations while providing insight into the biomolecular mechanism of respiratory chain failure. It should be noted that full-mtDNA PRS is possible using the 24-amplicon scheme of Rieder et al. and can be performed handily for a single individual on a single 96-lane μCAE device [10].

The observation of higher mutant populations in urine than in paired tumor, though not universal, is a common theme in these results. Intuition suggests that any cancer-associated mutation should be more readily detected in a carefully microdissected tumor sample than in the random collection of cells shed by the total urothelium, of whose cross-section the tumor presumably comprises only a small fraction. Nonetheless, equal or greater mutant representation in urine has been observed in our previous sequencing studies of matched tumor and bodily fluid [12, 13].

While mainstream sequencing techniques possess the ability to generate sequencing data in high volume, the sheer expanse of data and the lack of quantitative controls limit their performance in mutation detection, particularly in the context of genetically heterogeneous samples. Despite valiant efforts to address these concerns through high-performance quality-based data analysis [43], considerable hurdles remain in applying such conventional methodologies to high-sensitivity mutation analysis. In contrast, PRS employs a normal internal control to highlight differences in sequence character, thereby allowing for direct variant detection without the need for multiple trace analysis and manual sequence comparison. Moreover, the internal control affords heightened sensitivity to subtle differences in sequence, as evidenced by the heteroplasmic transition at G200 in sample 2. While striking in urine, this particular variation is weak in the tumor and would likely have been missed by conventional sequencing, in which a 25 % signal intensity cutoff is commonly employed for base calling purposes. Additionally, PRS requires minimal data processing, thereby preserving a maximal amount of raw data while eliminating the need for statistical modeling. The use of an internal standard derived from the individual's own germline also circumvents comparison to an arbitrary sequence standard such as the revised Cambridge reference mtDNA sequence, an algorithm commonly built into microarray analysis scripts. Consequently, authentic somatic mutants are identified cleanly without the confounding influence of deviation from an "expected" germline.

As cancer therapy enters an age of personalized healthcare, the requirement of accuracy in comparative sequencing technology will be paramount in ensuring proper diagnosis and treatment. The common PHRED-20 standard in conventional sequencing corresponds to 99 % confidence in a particular base call. Translated to sequence accuracy, this standard permits an unacceptable 17 errors per individual in the span of sequence analyzed here. Indeed, these concerns rise in concurrence with recent phylogenetic studies indicating high error rates in published sequencing-based mutation studies [44]. In addition to addressing these concerns through rigorous controls and quantitation, PRS presents the opportunity to interpret genetic heterogeneity, either in the context of mitochondrial heteroplasmy, as observed here, or in the analysis of potentially heterogeneous tissue, as is observed in tumor margins. A somatic mutation reliably linked to a particular cancer may therefore be exploited by PRS as an indicator of tumor invasion and used to define margins either prior to or during excision. Such an approach is applicable to any variant for which flanking primers are known, enlisting a library of thousands of potential markers. Coupled with the small sample sizes and rapid analysis times enabled by microchip analysis, a variety of key genes may be analyzed in parallel, elucidating the complete and unique genetic signatures of individual cancers at minimal cost. Integration of massively parallel μCAE separation technology with upstream PRS labeling and purification processes [44–46] will ultimately foster more rapid and facile analyses, while further integration with emerging technology for single-copy genetic analysis [47] may ultimately enable real-time cancer pathology at the individual cellular level.

Acknowledgments

The authors gratefully acknowledge Nadia Del Bueno, Samantha Cronier, Numrin Thaitrong, Jim Scherer, Peng Liu, and Kanwar Singh for valuable consultation. The involvement of Jing Yi and Terry Speed from the UC

Berkeley Statistics Department was central to the design of the automated PRS analysis software. Microfabrication was performed by Eric Chu at the UC Berkeley Microlab. This work was supported by NIH grants #HG03329, #CA77664, and #CA075115 (R.A.M.) and the University of Texas Health Science Center at Tyler, Texas (S.D.).

References

1. Jiang X, Wang X (2004) Cytochrome C-mediated apoptosis. Annu Rev Biochem 73:87–106 [PubMed: 15189137]
2. Warburg O (1956) On the origin of cancer cells. Science 123:309–314 [PubMed: 13298683]
3. Chatterjee A, Dasgupta S, Sidransky D (2011) Mitochondrial subversion in cancer. Can Prev Res 4:638–654
4. Dasgupta S, Hoque MO, Upadhyay S, Sidransky D (2008) Mitochondrial cytochrome B gene mutation promotes tumor growth in bladder cancer. Cancer Res 68:700–706 [PubMed: 18245469]
5. Ishikawa K, Takenaga K, Akimoto M, Koshikawa N, Yamaguchi A, Imanishi H, Nakada K, Honma Y, Hayashi J (2008) ROS-generating mitochondrial DNA mutations can regulate tumor cell metastasis. Science 320:661–664 [PubMed: 18388260]
6. Dasgupta S, Soudry E, Mukhopadhyay N, Shao C, Yee J, Lam S, Lam W, Zhang W, Gazdar AF, Fisher PB et al. (2012) Mitochondrial DNA mutations in respiratory complex-I in never-smoker lung cancer patients contribute to lung cancer progression and associated with EGFR gene mutation. J Cell Physiol 227:2451–2460 [PubMed: 21830212]
7. Wallace DC (2005) A mitochondrial paradigm of metabolic and degenerative diseases, aging, and cancer: a dawn for evolutionary medicine. Annu Rev Genet 39:357–407
8. Kujoth GC, Leeuwenburgh C, Prolla TA (2006) Mitochondrial DNA mutations and apoptosis in mammalian aging. Cancer Res 66:7386–7389 [PubMed: 16885331]
9. Mecocci P, MacGarvey U, Beal MF (1994) Oxidative damage to mitochondrial DNA is increased in Alzheimer's disease. Ann Neurol 36:747–751 [PubMed: 7979220]
10. Blazej RG, Paegel BM, Mathies RA (2003) Polymorphism ratio sequencing: a new approach for single nucleotide polymorphism discovery and genotyping. Genome Res 13:287–293 [PubMed: 12566407]
11. www.cancer.gov. Data accessed 11 November 2015
12. Fliss MS, Usadel H, Caballero OL, Wu L, Buta MR, Eleff SM, Jen J, Sidransky D (2000) Facile detection of mitochondrial DNA mutations in tumors and bodily fluids. Science 287:2017–2019 [PubMed: 10720328]
13. Dasgupta S, Shao C, Keane TE, Duberow DP, Mathies RA, Fisher PB, Kiemeney LA, Sidransky D (2012) Detection of mitochondrial DNA alterations in urine from urothelial cell carcinoma patients. Int J Cancer 131:158–164 [PubMed: 21826645]
14. Simpson PC, Roach D, Woolley AT, Thorsen T, Johnston R, Sensabaugh GF, Mathies RA (1998) High-throughput genetic analysis using microfabricated 96-sample capillary array electrophoresis microplates. Proc Natl Acad Sci USA 95:2256–2261 [PubMed: 9482872]
15. Paegel BM, Emrich CA, Wedemayer GJ, Scherer JR, Mathies RA (2002) High throughput DNA sequencing with a microfabricated 96-lane capillary array electrophoresis bioprocessor. Proc Natl Acad Sci USA 99:574–579 [PubMed: 11792836]
16. Woolley AT, Sensabaugh GF, Mathies RA (1997) High-speed DNA genotyping using microfabricated capillary array electrophoresis chips. Anal Chem 169:2181–2186
17. Mithani SK, Taube JM, Zhou S, Smith IM, Koch WM, Westra WH, Califano JA (2007) Mitochondrial mutations are a late event in the progression of head and neck squamous cell cancer. Clin Cancer Res 13:4331–4335 [PubMed: 17671113]
18. Hoque MO, Lee J, Begum S, Yamashita K, Engles JM, Schoenberg M, Westra WH, Sidransky D (2003) High-throughput molecular analysis of urine sediment for the detection of bladder cancer by high-density single-nucleotide polymorphism array. Cancer Res 63:5723–5726 [PubMed: 14522891]
19. Rieder MJ, Taylor SL, Tobe VO, Nickerson DA (1998) Automating the identification of DNA variations using quality-based fluorescence re-sequencing: analysis of the human mitochondrial genome. Nucleic Acids Res 26:967–973 [PubMed: 9461455]

20. Ju J, Ruan C, Fuller CW, Glazer AN, Mathies RA (1995) Fluorescence energy transfer dye-labeled primers for DNA sequencing and analysis. Proc Natl Acad Sci USA 92:4347–4351 [PubMed: 7753809]
21. Hjertén S (1985) High-performance electrophoresis: elimination of electroendosmosis and solute adsorption. J Chromatog 347:191–198
22. Scherer JR, Paegel BM, Wedemayer GJ, Emrich CA, Lo J, Medintz IL, Mathies RA (2001) High-pressure gel loader for capillary array electrophoresis microchannel plates. Biotechniques 31:1150–1152 [PubMed: 11730021]
23. Shi Y, Simpson PC, Scherer JR, Wexler D, Skibola C, Smith MT, Mathies RA (1999) Radial capillary array electrophoresis microplate and scanner for high-performance nucleic acid analysis. Anal Chem 71:5354–5361 [PubMed: 10596215]
24. Woolley AT, Hadley D, Landre P, deMello AJ, Mathies RA, Northrup MA (1996) Functional integration of PCR amplification and capillary electrophoresis in a microfabricated DNA analysis device. Anal Chem 68:4081–4086 [PubMed: 8946790]
25. Thaitrong N, Toriello NM, Del Bueno N, Mathies RA (2009) Polymerase chain reaction-capillary electrophoresis genetic analysis microdevice with in-line affinity capture sample injection. Anal Chem 81:1371–1377 [PubMed: 19140739]
26. Toriello NM, Liu CN, Blazej RG, Thaitrong N, Mathies RA (2007) Integrated affinity capture, purification, and capillary electrophoresis microdevice for quantitative double-stranded DNA analysis. Anal Chem 79:8549–8556 [PubMed: 17929900]
27. Emrich CA, Tian H, Medintz IL, Mathies RA (2002) Microfabricated 384-lane capillary array electrophoresis bioanalyzer for ultrahigh-throughput genetic analysis. Anal Chem 74:5076–5083 [PubMed: 12380833]
28. Ruiz-Pesini E, Lott MT, Procaccio V, Poole JC, Brandon MC, Mishmar D, Yi C, Kreuziger J, Baldi P, Wallace DC (2007) An enhanced MITOMAP with a global mtDNA mutational phylogeny. Nucleic Acids Res 35(Database issue):D823–D828, http://www.mitomap.org/ [PubMed: 17178747]
29. Williams C, Pontén F, Moberg C, Söderkvist P, Uhlén M, Pontén J, Sitbon G, Lundeberg J (1999) A high frequency of sequence alterations is due to formalin fixation of archival specimens. Am J Pathol 155:1467–1471 [PubMed: 10550302]
30. Andrews RM, Kubacka I, Chinnery PF, Lightowlers RN, Turnbull DM, Howell N (1999) Reanalysis and revision of the Cambridge reference sequence for human mitochondrial DNA. Nat Genet 23:147 [PubMed: 10508508]
31. Sun W, Zhou S, Chang SS, McFate T, Verma A, Califano JA (2009) Mitochondrial mutations contribute to HIF1α accumulation via increased reactive oxygen species and up-regulated pyruvate dehydrogenease kinase 2 in head and neck squamous cell carcinoma. Clin Cancer Res 15:476–484 [PubMed: 19147752]
32. Zhou S, Kachhap S, Sun W, Wu G, Chuang A, Poeta L, Grumbine L, Mithani SK, Chatterjee A, Koch W et al. (2007) Frequency and phenotypic implications of mitochondrial DNA mutations in human squamous cell cancers of the head and neck. Proc Natl Acad Sci USA 104:7540–7545 [PubMed: 17456604]
33. Tan DJ, Bai RK, Wong LJC (2002) Comprehensive scanning of somatic mitochondrial DNA mutations in breast cancer. Cancer Res 62:972–976 [PubMed: 11861366]
34. Nagy A, Wilhelm M, Sükösd F, Ljungberg B, Kovacs G (2002) Somatic mitochondrial DNA mutations in human chromophobe renal cell carcinomas. Genes Chromosomes Cancer 35:256–260 [PubMed: 12353267]
35. Polyak K, Li Y, Zhu H, Lengauer C, Willson JK, Markowitz SD, Trush MA, Kinzler KW, Vogelstein B (1998) Somatic mutations of the mitochondrial genome in human colorectal tumours. Nat Genet 20:291–293 [PubMed: 9806551]
36. Hibi K, Nakayama H, Yamazaki T, Takase T, Taguchi M, Kasai Y, Ito K, Akiyama S, Nakao A (2001) Detection of mitochondrial DNA alterations in primary tumors and corresponding serum of colorectal cancer patients. Int J Cancer 94:429–431 [PubMed: 11745425]

37. Jones JB, Song JJ, Hempen PM, Parmigiani G, Hruban RH, Kern SE (2001) Detection of mitochondrial DNA mutations in pancreatic cancer offers a “mass”-ive advantage over detection of nuclear DNA mutations. Cancer Res 61:1299–1304 [PubMed: 11245424]

38. Wong LJC, Lueth M, Li XN, Lau CC, Vogel H (2003) Detection of mitochondrial DNA mutations in the tumor and cerebrospinal fluid of medulloblastoma patients. Cancer Res 63:3866–3871 [PubMed: 12873974]

39. Jakupciak JP, Wang W, Markowitz ME, Ally D, Coble M, Srivastava S, Maitra A, Barker PE, Sidransky D, O’Connell CD (2005) Mitochondrial DNA as a cancer biomarker. J Mol Diagn 7:258–267 [PubMed: 15858150]

40. Liu VW, Shi HH, Cheung AN, Chiu PM, Leung TW, Nagley P, Wong LC, Ngan HY (2001) High incidence of somatic mitochondrial DNA mutations in human ovarian carcinomas. Cancer Res 61:5998–6001 [PubMed: 11507041]

41. Mithani SK, Smith IM, Topalian SL, Califano JA (2008) Nonsynonymous somatic mitochondrial mutations occur in the majority of cutaneous melanomas. Melanoma Res 18:214–219 [PubMed: 18477896]

42. Philley JV, Kannan A, Qin W, Sauter ER, Ikebe M, Hertweck KL, Troyer DA, Semmes OJ, Dasgupta S (2016) Complex-I alteration and enhanced mitochondrial fusion are associated with prostate cancer progression. J Cell Physiol 231:1364–1374 [PubMed: 26530043]

43. Nickerson DA, Tobe VO, Taylor SL (1997) PolyPhred: automating the detection and genotyping of single nucleotide substitutions using fluorescence-based resequencing. Nucleic Acids Res 25:2745–2751 [PubMed: 9207020]

44. Salas A, Yao YG, Macaulay V, Vega A, Carracedo A, Bandelt HJ (2005) A critical reassessment of the role of mitochondria in tumorigenesis. PLoS Med 2:e296 [PubMed: 16187796]

45. Blazej RG, Kumaresan P, Mathies RA (2006) Microfabricated bioprocessor for integrated nanoliter-scale Sanger DNA sequencing. Proc Natl Acad Sci USA 103:7240–7245 [PubMed: 16648246]

46. Blazej RG, Kumaresan P, Cronier SA, Mathies RA (2007) Inline injection microdevice for attomole-scale Sanger DNA sequencing. Anal Chem 79:4499–4506 [PubMed: 17497827]

47. Kumaresan P, Yang CJ, Cronier SA, Blazej RG, Mathies RA (2008) High-throughput single copy DNA amplification and cell analysis in engineered nanoliter droplets. Anal Chem 80:3522–3529 [PubMed: 18410131]

Key messages

- PRS accurately detects high mtDNA mutations in UCCs and their body fluids.
- mtDNA mutations are universally heteroplasmic and often appear at low levels.
- The PRS technology could be a viable approach to develop mitochondrial biomarkers.

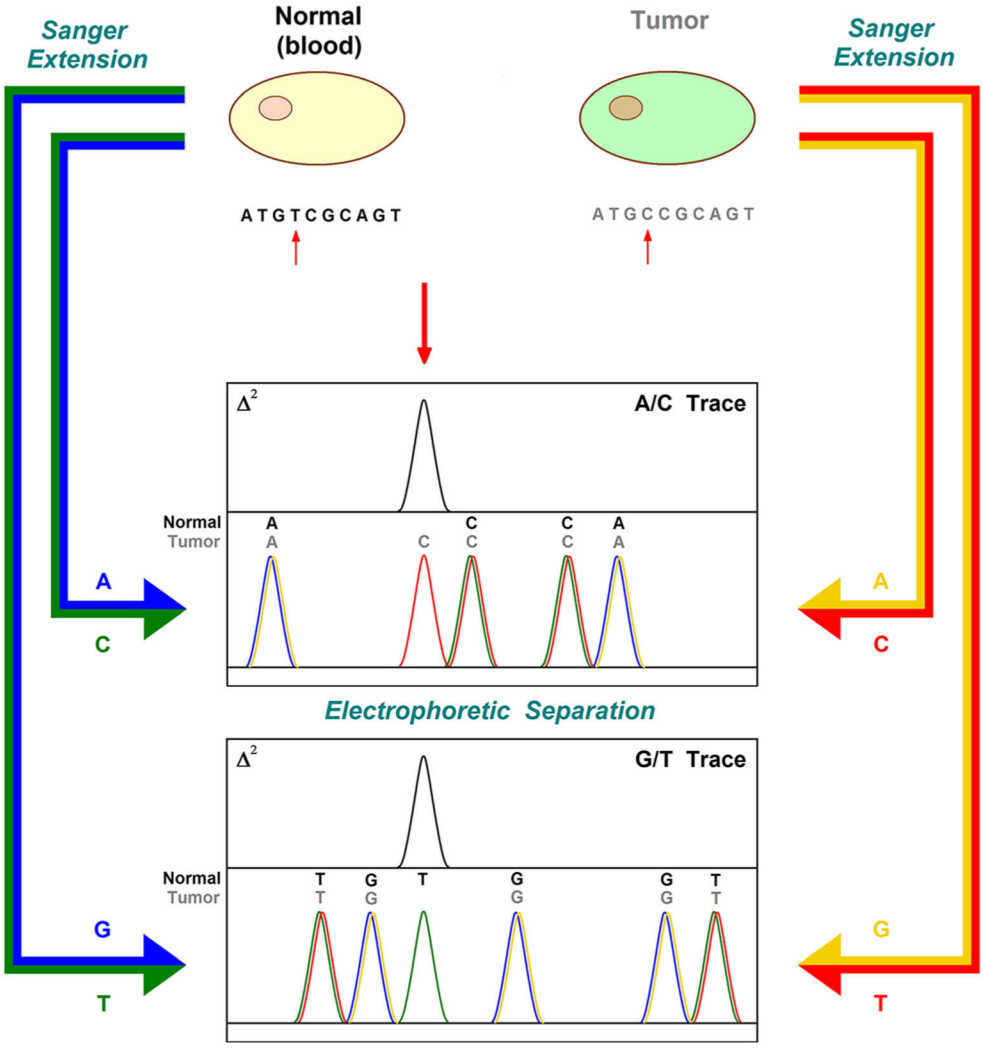

Fig. 1.

PRS labeling and pooling scheme for the detection of tumor mutations. Like-terminating bases from normal and tumor samples are independently Sanger-extended and labeled with differing dye primers to identify the template. Extension fragments are then pooled in two four-color-compatible mixtures (by convention, A/C and G/T) and separated, yielding electropherograms with perfect two-color overlap, except in regions of variation. Mutations are readily detected as single peaks in a squared difference plot and characterized based on the four-color peak signature. In this case, a T→C transition is identified as a lone “T normal” (*green*) peak in the G/T trace and a corresponding lone “C tumor” (*red*) peak in the A/C trace

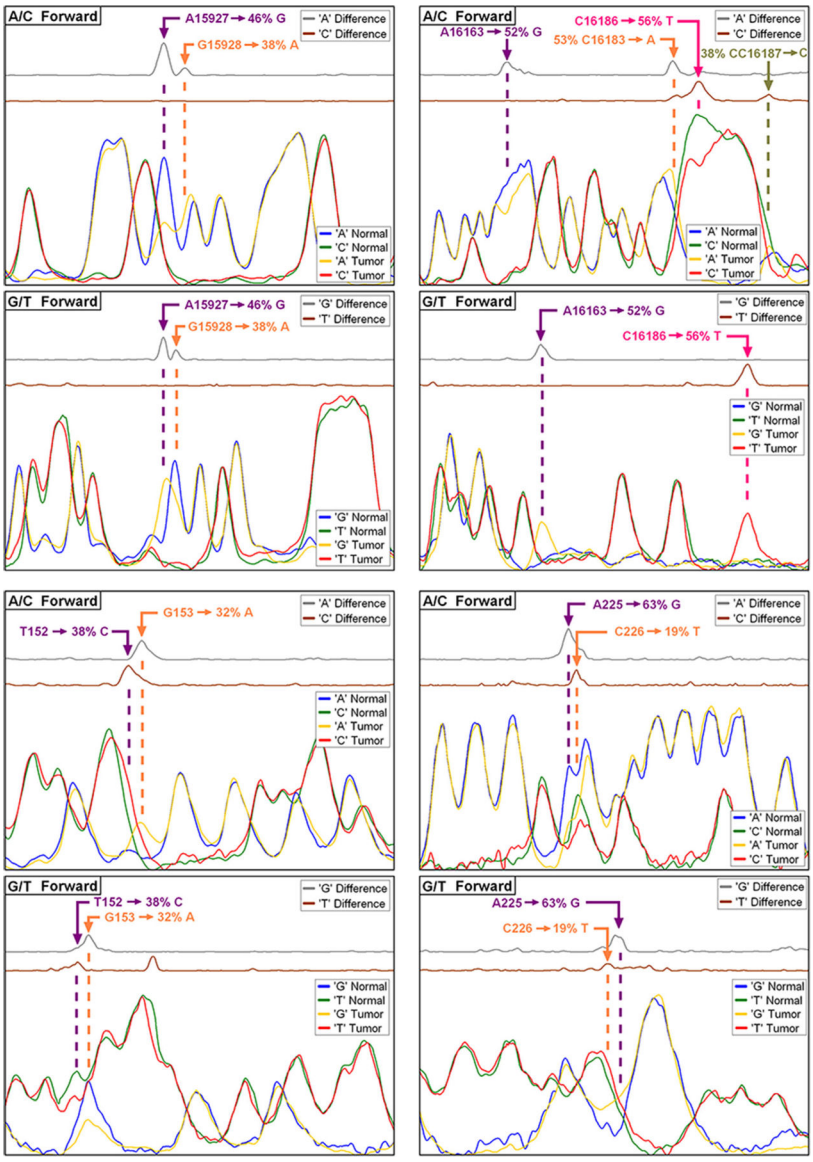

Fig. 2.

Selected PRS data from the highly mutant sample 6 (normal/tumor). Mutations detected in this sample were universally heteroplasmic and largely grouped into mutation clusters, such as those illustrated here. Mutant locations are identified by the difference traces for the affected bases, while the combined four-color peak signatures of A/C and G/T traces indicate the specific nature and degree of the change

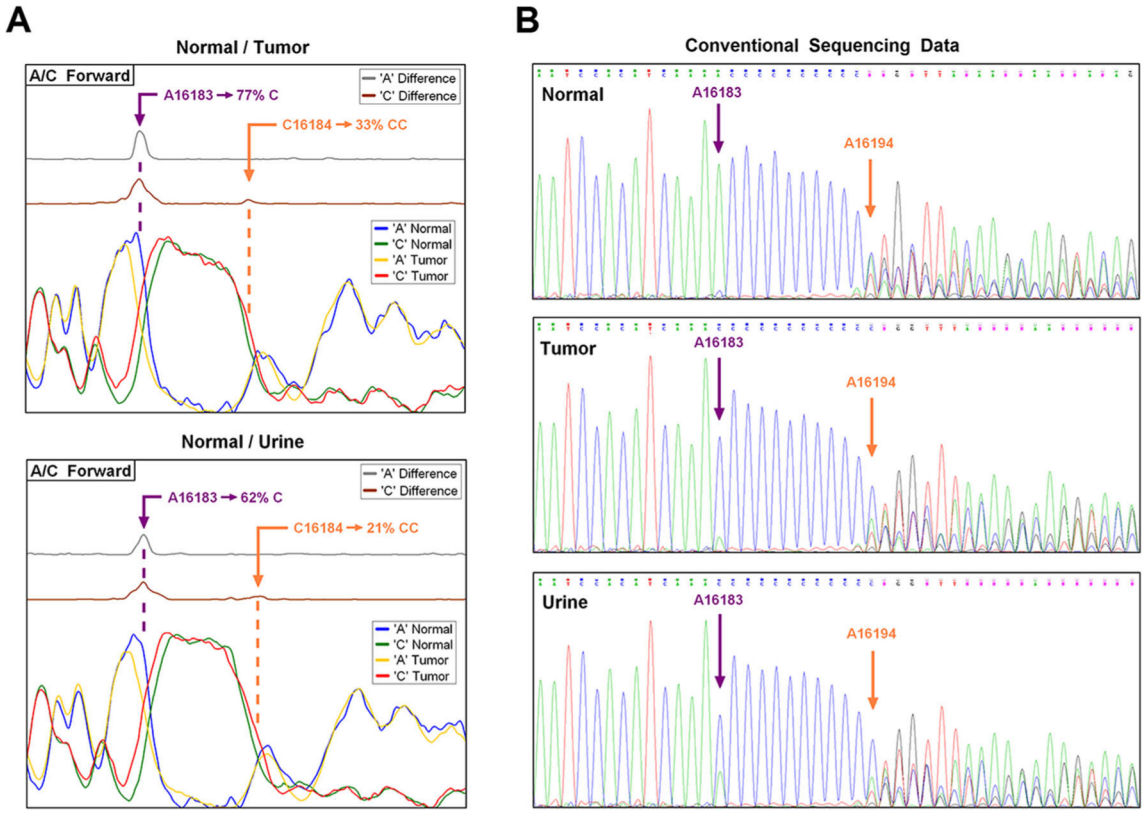

Fig. 3.

a Representative PRS data from sample 3 containing both the A→C transversion at 16183 and the C insertion at 16184. **b** Conventional sequencing confirms heteroplasmic changes at both positions, with all C-insertion character distributed among five distinct populations in normal and three in tumor and urine. These genetic populations are traceable by the rise and fall in *green* A16194 peaks following the repeat

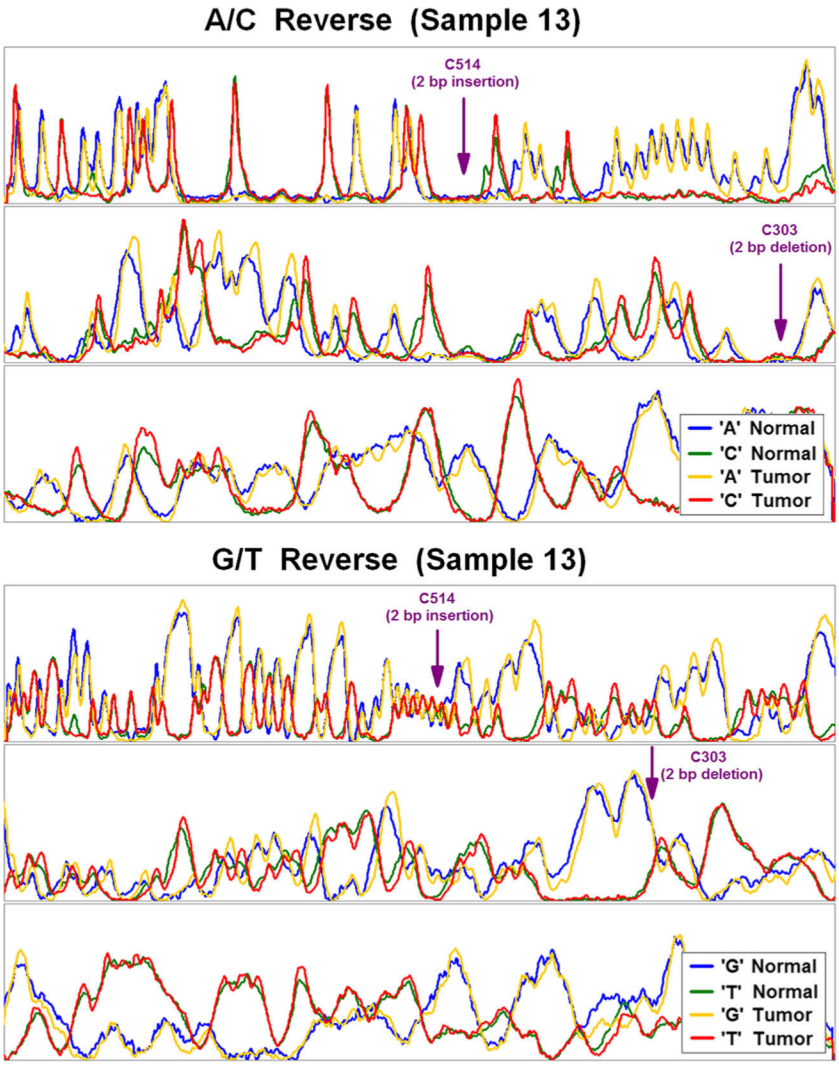

Fig. 4.

Double heteroplasmic insertion/deletion in sample 13. A two-base splitting of all normal traces after C514 indicates a heteroplasmic germline, with 79 % of lymphocyte mtDNA harboring a two-base insertion at this position (514: 21%C→CAC). The absence of splitting in the tumor traces indicates a somatic shift toward the dominant germline population, producing near-homoplasmy in the tumor. Normal and tumor traces are almost perfectly realigned at C303 by a heteroplasmic two-base deletion in the tumor (303: CCC→63%C)

Table 1

Compiled D-loop mutation results

Sample	Nucleotide position	Normal (lymphocyte)	Tumor	Urine
1	16184	C	42 % CC[a]	62 % CC[a]
2	200	G	6 % A	32 % A
	303	CC	36 % C[a]	80 % C[a]
3	16183	A	77 % C[a]	62 % C[a]
	16184	C	33 % CC[a]	21 % CC[a]
4	16184	C	50 % CCC[a]	62 % CCC[a]
6	152	T	38 % C	–
	153	G	32 % A	–
	225	A	63 % G	–
	226	C	19 % T	–
	303	43 % CC[a]	C	–
	15927	A	46 % G	–
	15928	G	38 % A	–
	16126	T	51 % C	–
	16163	A	42 % G[a]	–
	16183	56 % C[a]	A	–
	16186	C	56 % T	–
	16187	38 % CC[a]	C	–
	16223	T	51 % C[a]	–
	16278	T	45 % C	–
	16294	C	40 % T[a]	–
8	16223	T	95 % C	–
10	16184	C	72 % CCC[a]	–
13	303	CCC	63 % C[a]	–
	514	21 % C	CAC	–
	16092	5 % C	T	–
	16189	24 % C	T	–
	16192	27 % C	T	–

Unquantified base calls are 100 % within detection sensitivity

[a]Estimated populations for mutations occurring in low-resolution mononucleotide repeat regions. A total of 28 somatic variants were detected in 8 of 14 samples. All variants exhibit some degree of heteroplasmy, and seven represent population shifts from a heteroplasmic germline. All mutations detected in individuals with available urine DNA were readily detected in the bodily fluid